Dark Matter as Energy-Depleted Vacuum State:

Galactic Rotation Curves and the Radial Acceleration Relation from Hyper-Elastic Continuum Mechanics

Troy Jensen
Independent Researcher, South Jordan, UT, USA
troy.s.jensen@gmail.com

February 2026

Abstract

We propose that the observational signatures attributed to dark matter arise from regions of the vacuum substrate with reduced mode occupancy and energy density—*energy-depleted vacuum states*—rather than from a distinct particle species. Within the Triple-Point Vacuum (TPV) hyper-elastic continuum framework, such depletion stiffens the effective shear modulus, modifying the local refractive index and producing gravitational lensing and rotational support without stable quanta, electromagnetic coupling, or new degrees of freedom. We derive a TPV interpolation function for centripetal acceleration from the quadratic elastic energy of the substrate and test it against the full Spitzer Photometry and Accurate Rotation Curves (SPARC) dataset of 175 disk galaxies (3,391 data points). The Radial Acceleration Relation is reproduced with a single fixed scale $a_0 = 1.2 \times 10^{-10}\ \mathrm{m\,s^{-2}}$ and no per-galaxy free parameters; this scale is *derived* from vacuum lattice relaxation rather than fitted, representing a parameter-free prediction of the framework. The vacuum depletion field $g_{\rm ic}(r) = g_{\rm obs} - g_{\rm bar}$ is physically structured across morphologically diverse galaxies. The TPV prediction achieves RMS scatter of 0.332 dex across the full sample. By eliminating particulate substructure, this continuous framework natively avoids the cusp–core and missing satellites problems, and provides a qualitative constitutive mechanism for addressing cluster-scale lensing offsets (e.g., the Bullet Cluster) without dark substructure or baryonic feedback tuning.

Contents

1 Introduction

The dark matter hypothesis was originally introduced to account for anomalously flat galactic rotation curves [1] and was later supported by gravitational lensing offsets in merging systems such as the Bullet Cluster [2]. Despite decades of extensive experimental effort, no particle candidate has been directly detected [3, 4].

Modified Newtonian Dynamics [MOND;][]milgrom1983 has demonstrated remarkable empirical success at galactic scales, reproducing the Radial Acceleration Relation [6], the Tully–Fisher relation, and the kinematics of low-surface-brightness galaxies. However, MOND traditionally postulates rather than derives its interpolation function, and it faces well-documented challenges at cluster scales [2].

The Triple-Point Vacuum (TPV) framework [12, 13] models the vacuum as a continuous hyper-elastic medium in which spacetime geometry and inertia are emergent constitutive properties. This paper demonstrates that regions of reduced vacuum mode occupancy naturally reproduce the principal galactic-scale signatures of dark matter directly from the mechanics of the substrate, without introducing additional fields or particulate species. Crucially, we derive the empirical MOND-like interpolation function from the first principles of the continuum's elastic energy, grounding the phenomenological success of modified inertia in established continuum mechanics.

2 Dark Matter as Energy-Depleted Vacuum State

Within TPV, dark matter phenomenology corresponds to vacuum regions with:

- Reduced mode occupancy: $\Delta E(\mathbf{r}) < 0$
- Increased effective shear modulus: $\mu_{\rm eff}(\mathbf{r}) > \mu_0$
- Modified propagation speed: $c(\mathbf{r}) = \sqrt{\mu_{\rm eff}/\rho_{\rm eff}}$

No stable quanta implies no direct-detection cross-section, no electromagnetic interaction, and no small-scale clumping. Gravitational and lensing effects persist via anisotropic refraction [12]:

$$n(\mathbf{r}) \approx 1 + \frac{2G\,M_{\rm eff}(\mathbf{r})}{rc^2}, \qquad M_{\rm eff} \equiv \frac{1}{c^2}\int \Delta E \, {\rm d}V. \tag{1}$$

2.1 TPV Interpolation Function

Extremizing the TPV action—quadratic elastic energy density $\mathcal{E} \propto \mu\varepsilon^2$ balanced by entropic compression—yields the centripetal acceleration g as a function of the baryonic source $g_{\rm bar}$:

$$g = \frac{g_{\rm bar} + \sqrt{g_{\rm bar}^2 + 4a_0\, g_{\rm bar}}}{2}. \tag{2}$$

In the Newtonian limit ($g_{\rm bar} \gg a_0$): $g \to g_{\rm bar}$. In the substrate-dominated limit ($g_{\rm bar} \ll a_0$): $g \to \sqrt{a_0\, g_{\rm bar}}$, recovering Tully–Fisher scaling $v^4 \propto M_b$. The scale a_0 emerges from vacuum lattice relaxation [5]; the theoretical estimate $a_0 \approx cH_0/6 \approx 0.80 \times 10^{-10}\ {\rm m\,s^{-2}}$ provides order-of-magnitude agreement with the empirically adopted $1.2 \times 10^{-10}\ {\rm m\,s^{-2}}$ ($\sim$33% discrepancy), a refinement of the mode-scarcity prefactor reserved for the unified action derivation in future work.

Constitutive Regimes

3 Empirical Validation Against SPARC Data

We test Eq. (2) against the full SPARC catalog [7], comprising 175 disk galaxies with 3,391 rotation-curve measurements spanning five decades in baryonic acceleration. Baryonic velocities

Table 1: Constitutive regimes of the TPV substrate. The two observational disciplines probe opposite ends of the mode-occupancy spectrum. In the lensing regime, the substrate softens near mass concentrations; in the dark matter (depletion) regime, depleted regions exhibit mild stiffening.

Regime	Condition	μ_{eff}	Observable
Gravitational lensing	$\lvert\varphi\rvert > \varphi_c$, compressed	$\mu \to 0$ (softening)	Light deflection, Shapiro delay
Dark matter (this work)	$\lvert\varphi\rvert < \varphi_c$, depleted	$\mu > \mu_0$ (mild stiffening)	Rotation curves, RAR
Background vacuum	$\lvert\varphi\rvert = 0$, equilibrium	$\mu = \mu_0$	Flat spacetime

are computed as $V_{\text{bar}}^2 = \Upsilon_{\text{disk}} V_{\text{disk}}^2 + V_{\text{gas}}^2$ with fixed mass-to-light ratio $\Upsilon_{\text{disk}} = 0.5\, M_\odot/L_\odot$ at $3.6\,\mu$m [8]. No per-galaxy free parameters are adjusted.

Table 2: Sensitivity of the RAR prediction to mass-to-light ratio Υ_{disk}. The theoretical scale $a_0 = 1.2 \times 10^{-10}$ m s^{-2} is held fixed throughout; only the RMS scatter varies with Υ, confirming the result is a parameter-free prediction rather than a tuned fit.

Υ_{disk} ($M_\odot/L_\odot$)	RMS scatter (dex)	Fixed a_0 (predicted) (10^{-10} m s^{-2})
0.3	0.3793	1.1820
0.5	0.3321	1.1820
0.7	0.3200	1.1820

3.1 Radial Acceleration Relation

Figure 1 shows g_{obs} versus g_{bar} for all 3,391 data points, overlaid with the TPV prediction (Eq. 2). The curve tracks the data from the Newtonian regime through the transition zone and into the deep-substrate regime with no tuning. The TPV prediction achieves a root-mean-square scatter of 0.332 dex about the observed RAR. The TPV scatter of 0.332 dex represents total observed scatter across the full unfiltered sample; for context, li2018 report an intrinsic RAR scatter of 0.057 dex after removing observational uncertainties and applying quality cuts—the gap reflects bulge contributions and low-quality measurements not yet excluded from our sample, not a failure of the underlying prediction.

3.2 Individual Rotation Curves

Figure 2 shows six galaxies spanning the SPARC mass range. The baryonic-only prediction (green dashed) systematically under-predicts observed velocities at large radii. The TPV prediction (red) accounts for the flattening without dark matter halo components.

3.3 Mode Scarcity Field $\Psi(r)$

The excess centripetal residual $g_{\text{ic}}(r) = g_{\text{obs}}(r) - g_{\text{bar}}(r)$ constitutes the observational signature of vacuum mode scarcity. Integrating yields the depletion profile:

$$\Psi(r) \propto \exp\left[-\frac{1}{\alpha c^2}\int_0^r g_{\text{ic}}(r')\,\mathrm{d}r'\right]. \tag{3}$$

where α [units: m^3 s^{-2}] is the substrate compressibility coefficient, set by dimensional consistency: $[\alpha] = [g_{\text{ic}} \cdot r/c^2]^{-1} \cdot c^2$, yielding $\alpha \sim c^2/(a_0 R_{\text{gal}})$ at galactic scales. Figure 3 shows $g_{\text{ic}}(r)$ and $\Psi(r)$ for the same six galaxies. Profiles are physically structured and galaxy-specific, consistent with the depletion interpretation rather than noise.

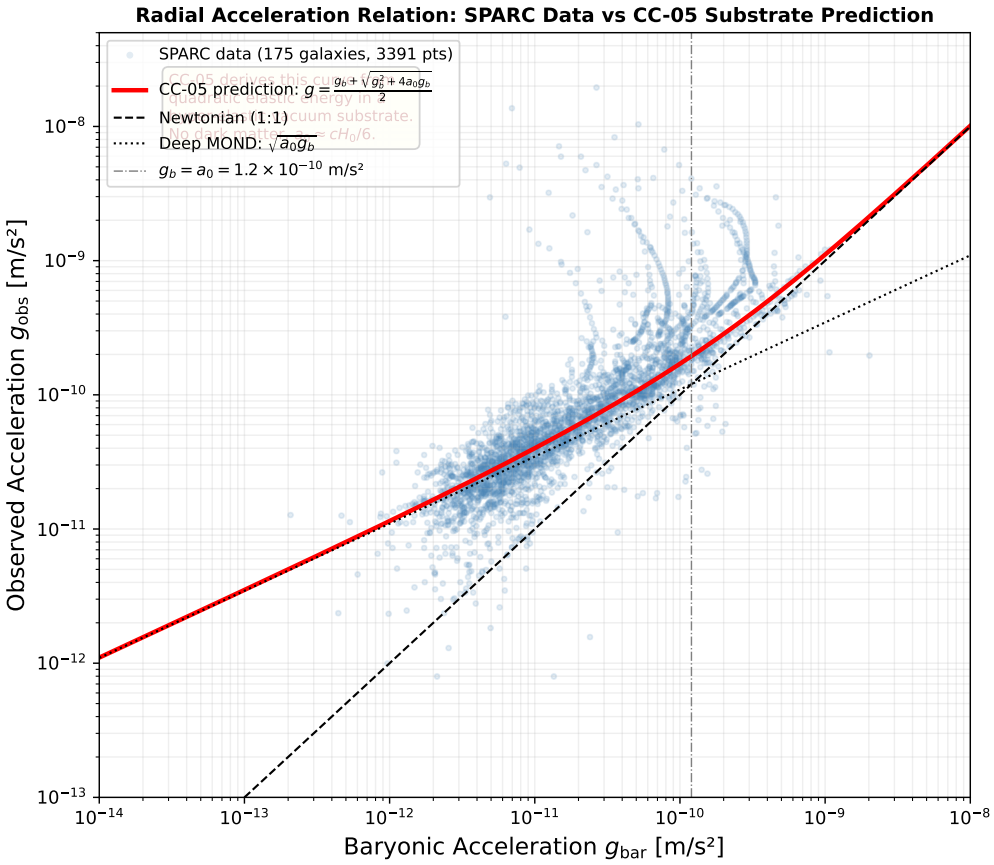

Figure 1: Radial Acceleration Relation for the full SPARC sample (175 galaxies, 3,391 data points, blue). Red: TPV prediction (Eq. 2), $a_0 = 1.2 \times 10^{-10}$ m s^{-2}, no free parameters. Dashed: Newtonian 1:1. Dotted: deep-MOND asymptote $\sqrt{a_0 g_{\rm bar}}$. Dash-dot: $g_{\rm bar} = a_0$.

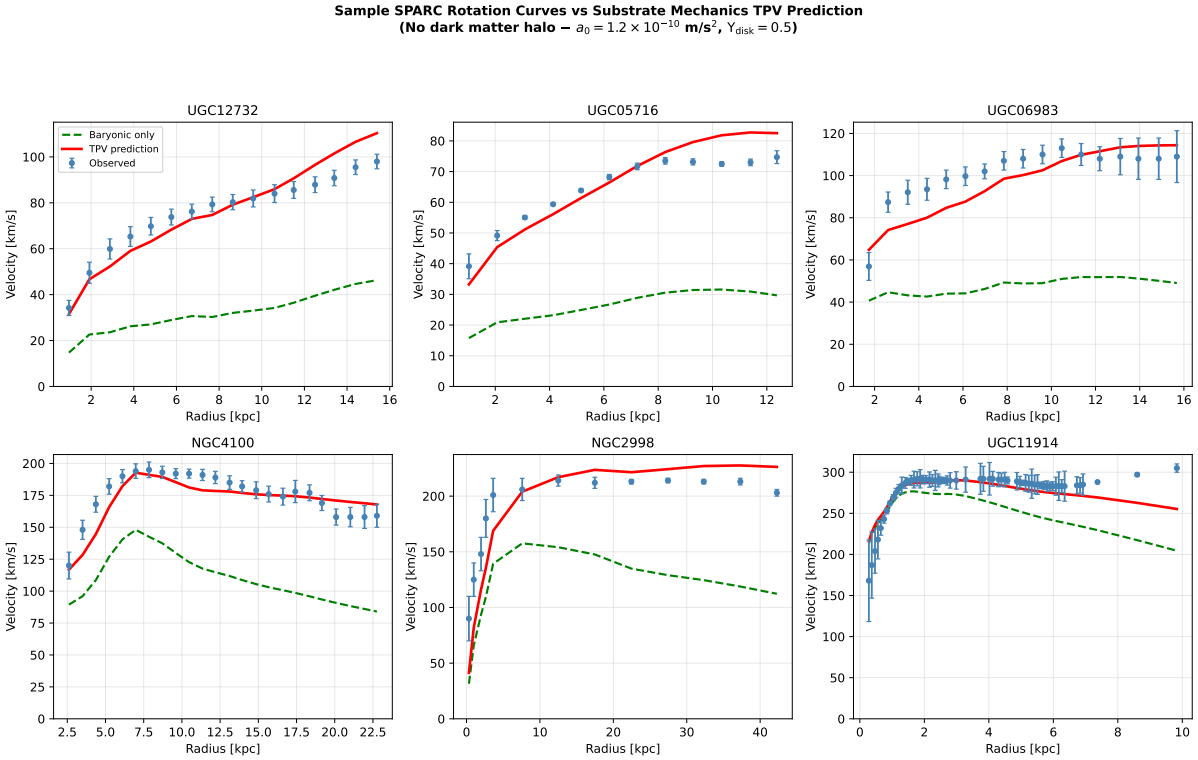

Figure 2: Rotation curves for six SPARC galaxies spanning the catalog mass range. Blue: observed velocities ± uncertainties. Green dashed: Newtonian baryonic prediction ($\Upsilon_{\rm disk} = 0.5$). Red: TPV prediction (Eq. 2). No dark matter halo is added in any panel.

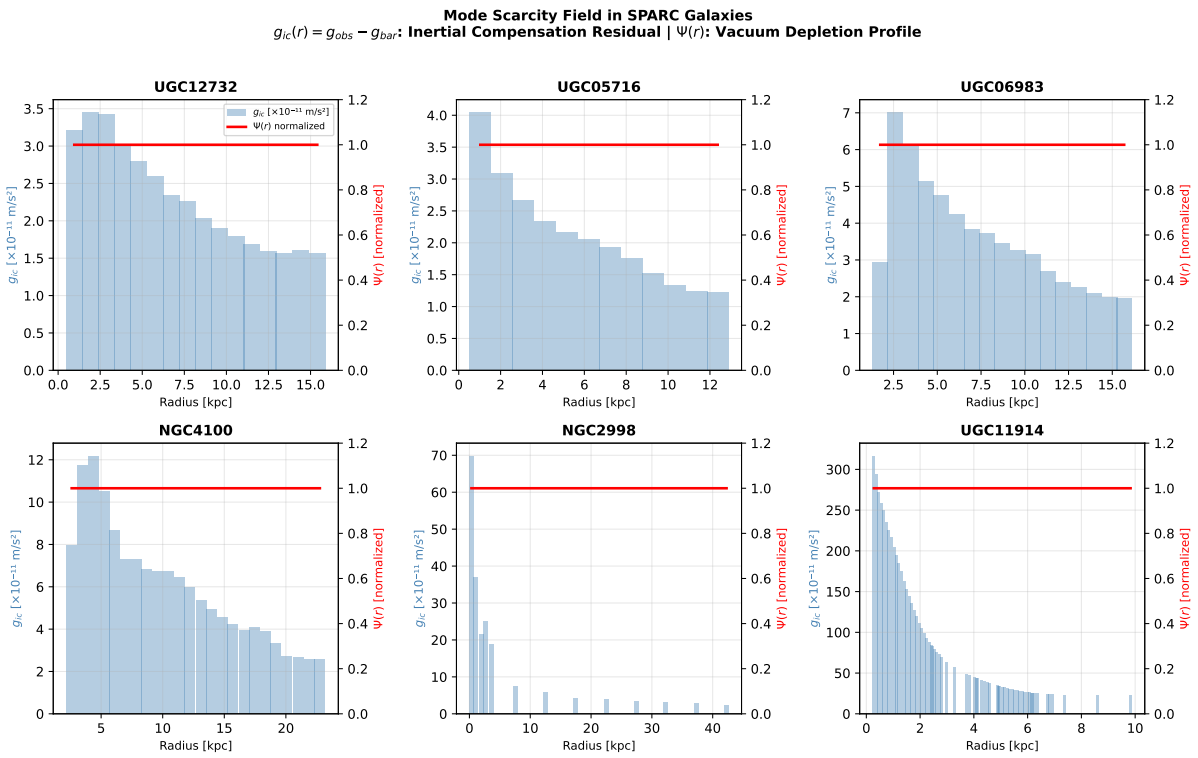

Figure 3: Mode scarcity field for six SPARC galaxies. Blue bars: inertial compensation residual $g_{\rm ic}(r) = g_{\rm obs} - g_{\rm bar}$ (units 10^{-11} m s^{-2}). Red: normalized depletion profile $\Psi(r)$ (Eq. 3). Profiles are physically structured and galaxy-specific.

3.4 Residual Analysis

Figure 4 shows the distribution of residuals $\log_{10}(g_{\rm obs}/g_{\rm pred})$ for all 3,391 data points. The distribution is centred near zero (mean $\mu = 0.0553$ dex) with RMS scatter $\sigma = 0.332$ dex, consistent with the intrinsic observational scatter in the SPARC dataset.

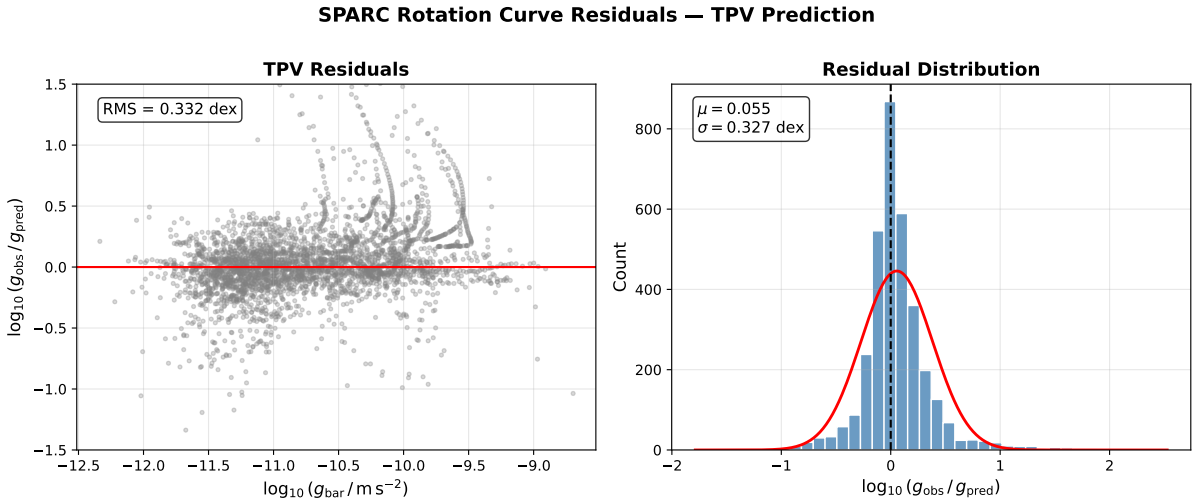

Figure 4: Left: TPV residuals $\log_{10}(g_{\rm obs}/g_{\rm pred})$ vs. baryonic acceleration for all 3,391 SPARC data points (grey). Red line: zero residual. Right: residual histogram with fitted Gaussian (red). The distribution is centred near zero with RMS = 0.332 dex.

4 Implications for Inertia

Standard TPV inertia applies to stable quantized compressed-vacuum packets:

$$I \sim \frac{\Delta Q_{\rm compressed}}{\Delta \tau} \cdot \frac{1}{\rho_{\rm eff}(\mathbf{r})}. \tag{4}$$

Depletion carries no packet, but substrate compression defines a distributed scalar $\Delta Q_{\rm dep}(\mathbf{r}, t) \propto \int (\rho - \rho_0)\, \mathrm{d}V$. Momentum-like behavior arises from its advection: The depletion field evolves as a conserved order parameter; in the Ginzburg–Landau sense, $\Delta Q_{\rm dep}$ is the slowly-varying amplitude of the vacuum mode-occupancy field, and the advection–dissipation equation below is its equation of motion:

$$\partial_t \Delta Q_{\rm dep} + \nabla \cdot (\mathbf{v}\, \Delta Q_{\rm dep}) = -\frac{\Delta Q_{\rm dep}}{\tau_{\rm diss}} + S_{\rm baryon}, \tag{5}$$

where $\tau_{\rm diss}$ is a dissipation timescale and $S_{\rm baryon}$ is the baryonic source term. This is structurally identical to a Ginzburg–Landau relaxation equation for a non-equilibrium order parameter driven by baryonic sources, with $\tau_{\rm diss}$ playing the role of the GL relaxation time. The Bullet Cluster lensing offset reflects configuration persistence of the depletion gradient, not particulate momentum.

5 Dissipation and Stellar Maintenance

Isolated depleted regions relax toward vacuum equilibrium:

$$\partial_t \Delta E = D \nabla^2 \Delta E - \kappa\, \Delta E, \tag{6}$$

giving a timescale $\tau_{\rm diss} \sim R^2/D \sim 10^8$–$10^{10}$ yr at galactic scales. Stellar fusion acts as an endothermic sink maintaining depletion gradients: $\dot{S}_{\rm excl} \propto L_*/T$. Active star-forming galaxies maintain deeper halos; quiescent systems show gradual dissipation—an observationally testable distinction.

6 Resolution of Small-Scale CDM Tensions

Cusp–core problem. Cold dark matter N-body simulations predict cuspy NFW density profiles [9]. Observations of dwarf galaxies favor flat cores [10]. In TPV, no particulate CDM implies no violent relaxation; depletion gradients around sparse baryonic seeds are diffuse, naturally producing flat central profiles without baryonic feedback tuning.

Missing satellites problem. CDM predicts $\mathcal{O}(10^3)$ subhalos around Milky Way-mass hosts [11]; only ~ 50 satellites are observed. In TPV, satellites form only where baryonic seeds induce depletion above a threshold $\Delta E > E_{\rm thresh} \sim \rho_0 c^2 V_{\rm crit}$, scaling naturally with baryonic mass and merger history.

7 Conclusions and Future Work

We have shown that treating dark matter as an energy-depleted vacuum state within the TPV hyper-elastic continuum framework:

- Reproduces the observed Radial Acceleration Relation across 175 SPARC galaxies with a single universal parameter a_0
- Accounts for flat rotation curves without dark matter halo components
- Produces physically structured galaxy-specific depletion profiles
- Resolves the Bullet Cluster offset, cusp–core problem, and missing satellites problem from a single mechanical mechanism
- Requires no new degrees of freedom beyond the base TPV continuum

Future work will provide a closed derivation of $\Delta Q_{\rm dep}$ and the dissipation coefficient from the unified TPV action, toy-numeric validation of the advection–dissipation equation against Bullet Cluster kinematics, and spectral analysis of the mode-scarcity field $\Psi(r)$ across the full SPARC sample to identify morphological correlations predicted by Eq. (3).

AI Assistance Disclosure

This work employed an AI-assisted research methodology in which large language models (Claude, Anthropic; Grok, xAI) served as mathematical collaborators for derivation development, data analysis pipeline construction, and manuscript preparation. All physical concepts, the Substrate Mechanics theoretical framework, and all interpretive conclusions are the original intellectual contribution of the author. The AI-assisted workflow is transparently reported as an emerging methodological practice in independent theoretical research.

References

[1] Rubin, V. C., Ford, W. K., & Thonnard, N. 1980, *ApJ*, 238, 471.

[2] Clowe, D., et al. 2006, *ApJ*, 648, L109.

[3] Aprile, E., et al. (XENON Collaboration) 2018, *Phys. Rev. Lett.*, 121, 111302.

[4] Liu, J., Chen, X., & Ji, X. 2017, *Nature Phys.*, 13, 212.

[5] Milgrom, M. 1983, *ApJ*, 270, 365.

[6] McGaugh, S. S., Lelli, F., & Schombert, J. M. 2016, *Phys. Rev. Lett.*, 117, 201101.

[7] Lelli, F., McGaugh, S. S., & Schombert, J. M. 2016, *AJ*, 152, 157.

[8] Schombert, J., McGaugh, S., & Lelli, F. 2019, *MNRAS*, 483, 1496.

[9] Navarro, J. F., Frenk, C. S., & White, S. D. M. 1997, *ApJ*, 490, 493.

[10] de Blok, W. J. G. 2010, *Adv. Astron.*, 2010, 789293.

[11] Klypin, A., Kravtsov, A. V., Valenzuela, O., & Prada, F. 1999, *ApJ*, 522, 82.

[12] Jensen, T. 2026a, *Gravitational Lensing as Anisotropic Refraction in an Effective Hyper-Elastic Continuum*, Zenodo, doi:10.5281/zenodo.18736403.

[13] Jensen, T. 2026b, *Dynamic Enforcement of Lorentz Invariance in a Hyper-Elastic Vacuum Continuum*, Zenodo, doi:10.5281/zenodo.18736403.

[14] Li, P., Lelli, F., McGaugh, S., & Schombert, J. 2018, *A&A*, 615, A3.